[1] P. Schwarzkopf, R. Kieffer, *Refractory Hard Metals: Borides, Carbides, Nitrides and Silicides*, MacMillan, New York **1953**.
[2] E. Fryt, *Solid State Ionics* **1997**, *101–103*, 437.
[3] N. Durlu, *J. Eur. Ceram. Soc.* **1999**, *19*, 2415.
[4] a) D. C. Halvalson, K. H. Ewald, Z. A. Munir, *J. Mater. Sci.* **1993**, *28*, 4583. b) D. Strzeciwilk, Z. Wokulski, P. Tkacz, *Cryst. Res. Technol.* **2003**, *38*, 283.
[5] D. D. Harbuck, C. F. Davidson, B. Monte, *J. Met.* **1986**, *38*, 47.
[6] D. W. Lee, B. K. Kim, *Scr. Mater.* **2003**, *48*, 1513.
[7] L. M. Berger, *J. Hard Mater.* **1992**, *3*, 3.
[8] R. Koc, J. S. Folmer, *J. Mater. Sci.* **1997**, *32*, 3101.
[9] C. Johnson, H. Sellinschegg, D. C. Johnson, *Chem. Mater.* **2001**, *13*, 3876.
[10] R. Koc, *J. Eur. Ceram. Soc.* **1997**, *17*, 1309.
[11] G. A. Swift, R. Koc, *J. Mater. Sci.* **1999**, *34*, 3083.
[12] L.-Q. Wang, Y. Shin, W. D. Samuels, G. J. Exarhos, I. L. Moudrakovski, V. V. Terskikh, J. A. Ripmeester, *J. Phys. Chem. B* **2003**, *107*, 13 793.
[13] Z. Jiang, W. E. Rhine, *Chem. Mater.* **1991**, *3*, 1132.
[14] H. Preiss, E. Schierhorn, K.-W. Brzezinka, *J. Mater. Sci.* **1998**, *33*, 4697.
[15] E. K. Storms, *The Refractory Carbides*, Refractory Materials Ser., Vol. 2, Academic Press, New York **1967**.
[16] Y. Shin, J. Liu, J. H. Chang, Z. Nie, G. J. Exarhos, *Adv. Mater.* **2001**, *13*, 728.
[17] T. Ota, M. Imeada, H. Takase, M. Kobayashi, N. Kinoshita, T. Hirashita, H. Miyazaki, Y. Hikichi, *J. Am. Ceram. Soc.* **2000**, *83*, 1521.

Mesoporous Single-Crystal ZnO Nanowires Epitaxially Sheathed with Zn_2SiO_4**

By *Xudong Wang*, *Christopher J. Summers*, and *Zhong Lin Wang**

Zinc oxide has been recognized as one of the most important semiconductor materials for optoelectronics[1] and piezoelectricity[2] effects because of its direct wide bandgap (3.37 eV) and non-centrosymmetric structure. Recently, intensive research has been focused on fabricating ZnO nanostructures and revealing their growth mechanisms and optical and electronic properties. A variety of ZnO nanostructure morphologies, such as nanobelts,[3] nanowires,[4] nanorods,[5] nanotubes,[6] and nanohelices/nanosprings[7] have been synthesized. Metal catalysts, such as gold[1,4,8] and tin[5,9,10] have been employed in the synthesis to align the structures,[1,4,5] confine them in size,[8,9] or to form junctions.[10] Applications of ZnO nanostructures are closely related to their morphology, and most of the ZnO nanostructures reported are dominated by the {0001}, $\{2\bar{1}\bar{1}0\}$, and $\{01\bar{1}0\}$ facets with solid walls/interiors.[11]

Porous materials have exhibited a wide variety of applications in bioengineering, catalysis, environmental engineering, and sensor systems, owing to their high surface-to-volume ratio. Normally, most mesoporous structures are composed of amorphous materials[12,13] and the porosity is achieved by solvent-based organic or inorganic reactions.[14] There are few reports of mesoporous structures based on crystalline materials.

In this paper, we report for the first time a new wurtzite ZnO nanowire structure that is single crystalline but composed of mesoporous walls/interiors. The highly porous ZnO nanowires were also enclosed by a thin layer of epitaxial Zn_2SiO_4 at the exterior surface, which was formed during synthesis performed with the use of a silicon substrate. A possible growth mechanism is proposed to understand the formation of the structure. These high-porosity single-crystal wire-like structures have potential applications as filters, catalyst supports, and gas sensors.

The synthesis is based on a modified solid–vapor process. The morphology of the porous ZnO nanowires is shown in Figure 1. Figure 1a is a low-magnification scanning electron

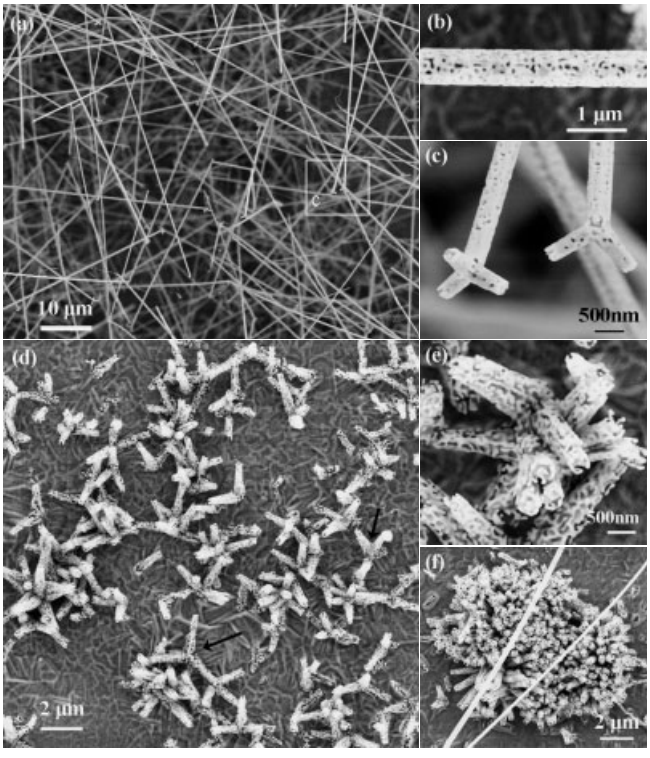

Figure 1. a) Low-magnification SEM image of high-porosity ZnO nanowires grown on a tin-coated silicon substrate; b) higher magnification SEM image showing the high-porosity morphology; c) a close-up view of the tetrapod structure; d) porous ZnO sprouts grown on a non-tin-covered region; e) a close view of the ZnO sprouts; f) partially aligned ZnO sprouts in the form of coral-like structure.

[*] Prof. Z. L. Wang, X. D. Wang, Prof. C. J. Summers
Center for Nanoscience and Nanotechnology
School of Materials Science and Engineering
Georgia Institute of Technology
Atlanta, GA 30332-0245 (USA)
E-mail: zhong.wang@mse.gatech.edu

[**] Thanks is expressed for the financial support from the US NSF grant DMR-9733160 and the MURI program from ARO (DAAD19-01-1-0603).

 DOI: 10.1002/adma.200306505

ADVANCED MATERIALS

microscopy (SEM) image of the as-synthesized ZnO nanowires deposited on a silicon substrate coated with a thin layer of tin to act as a catalyst for growth. The typical length of the nanowires varies from 100 μm to 1 mm and the diameter is in the range of 50–500 nm. The porous structure of the ZnO nanowires is shown more clearly in a high-magnification SEM image in Figure 1b, which display a hexagonal surface morphology. Moreover, most of the nanowires have the tetragonal configuration at the end as shown in Figure 1c.

On the silicon substrate surface not covered by tin, low-density ZnO tubular sprouts were found growing upwards from the silicon substrate as shown in Figure 1d. All of the sprouting tubes have about the same length and diameter and exhibit high-porosity walls/interiors (Fig. 1e). Most of the sprouting tubes retain the tetrapod structure, as indicated by arrowheads. Moreover, many sprouting tubes can grow together in tightly confined regions and form partially aligned ZnO coral structures as shown in Figure 1f, where the tetrapod structure is identified at the side of the coral structure.

Crossed structures consisting of two nanowires have also been observed (Fig. 2a). The porosity in the nanowire is apparent, and its hexagonal shape is clearly visible. Arrays of short nanowires (nanorods) have also been formed, as presented in Figure 2b, which have rib-like structures.

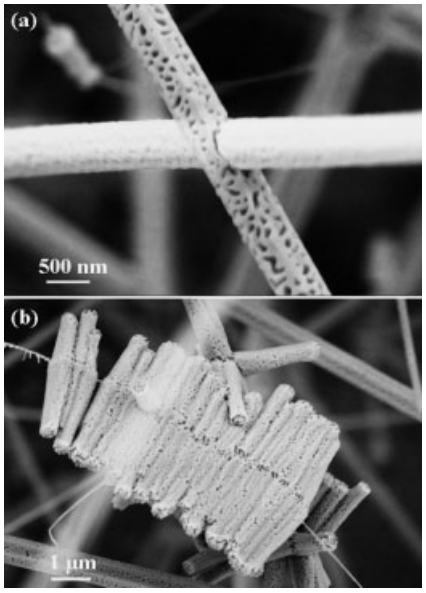

Figure 2. a) A junction between two porous ZnO nanowires; b) rib-like structure formed by aligning porous ZnO rods side-by-side on a nanowire.

Transmission electron microscopy (TEM) studies were carried out to examine the crystallography and the growth mechanism of the ZnO nanowires. The porous structure is clearly seen in the TEM image (Fig. 3a). A corresponding electron diffraction pattern recorded from the nanowire is shown in Figure 3b, but it presents two sets of patterns: the brighter spots come from ZnO, which is the $[2\bar{1}\bar{1}0]$ zone axis pattern, displaying the nanowire axial direction of [0001]; the weaker diffraction spots correspond to a different phase. A high-resolution TEM image recorded from the side of the nanowire shows that the phase is sheathed on the surface of the nanowire and has an epitaxial orientation related to ZnO. In Figure 3c, on the top of the ZnO crystal, which has a lattice fringe spacing of $c = 0.52$ nm perpendicular to the growth direction, a few fringes with a spacing of ~1 nm from the new phase are present and lie parallel to the wire axis.

Chemical analysis provides the first hint for defining the structure of the new phase. The energy-dispersive X-ray spectrum (EDS) (Fig. 3e) recorded from the edge of the nanowire shown in Figure 3d indicates the presence of Zn, Si, and O in the new phase. The atomic ratio of Si to Zn is about 2:3, smaller that than in Zn_2SiO_4, due to the presence of a thin silica layer on the surface of the nanowire. In reference to the real space interplanar distance of ZnO, the corresponding reflection planes of the new phase can be determined from the electron diffraction pattern presented in Figure 3b. The diffraction pattern from the new phase can be indexed to be the [100] zone axis of Zn_2SiO_4. The orientation relationship between ZnO and Zn_2SiO_4 is: $(0001)_{ZnO} \parallel (001)_{Zn_2SiO4}$, $[2\bar{1}\bar{1}0]_{ZnO} \parallel [100]_{Zn_2SiO4}$. Structurally, Zn_2SiO_4 has an orthorhombic crystal structure with lattice constants of $a = 0.9085$ nm, $b = 1.0625$ nm, and $c = 0.5962$ nm. Figure 3f is a high-resolution TEM image that clearly shows the formation of the Zn_2SiO_4 layer. A 20 nm thick layer on the bottom is clearly single-crystalline Zn_2SiO_4. Figure 3g shows the pure ZnO crystal lattice recorded at the end of the nanowire; the outer layer is shown in Figure 3h, which exhibits a pure Zn_2SiO_4 crystal structure surrounded by a thin layer of amorphous SiO_2.

The formation of the tetrapod structure presented in Figures 1c,d indicate that the solid ZnO nanowire is formed first. According to the Iwanaga model[15] (so-called octa-twin model),[16] the first homogeneous ZnO nuclei formed are octa-twins, and consist of eight tetrahedral-shape crystals, each consisting of three $\{11\bar{2}2\}$ pyramidal facets and one (0001) basal facet. The eight tetrahedral crystals are connected together by contacting the pyramidal faces with one another to form an octahedron. The surfaces of the octa-twins are all basal planes, but the eight basal surfaces of the octa-twin are alternately the Zn-terminated (0001) surfaces and the oxygen-terminated $(000\bar{1})$ surfaces. Since the (0001) surface is chemically active, while the $(000\bar{1})$ surface is inert,[17] the growth of nanowires along [0001] from the Zn-terminated (0001) surfaces results in the formation of the tetrapod. The four legs of each tetrapod structure are expected to have equivalent growth rates, at least during the early growth stage, as supported by the image in Figure 1d recorded from an area uncovered with tin catalyst. In the region covered with tin, the leg that is directly in contact with the tin catalyst on the substrate surface is likely to grow much faster, due to a vapor–liquid–solid growth mechanism occurring at the root (interface with the catalyst), than the legs that are grown by self-catalyzing[17] without the assistance of tin. This could cause the tetra-

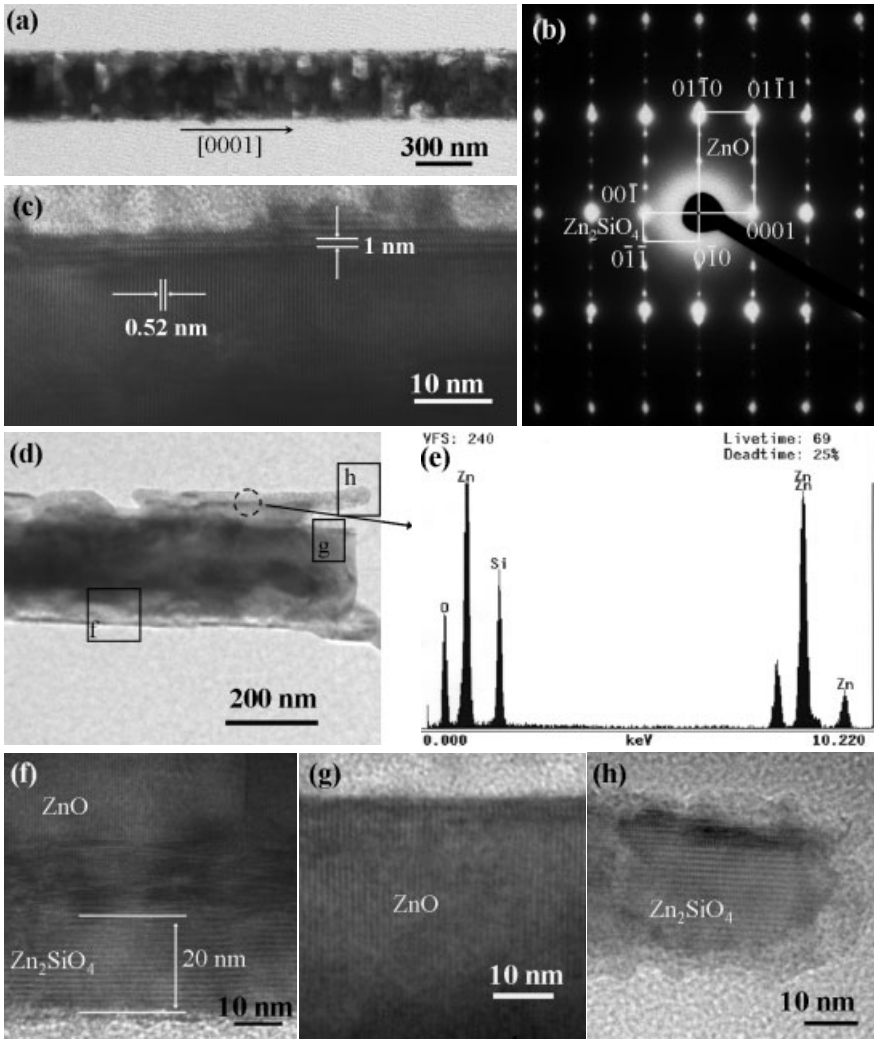

Figure 3. a) Low-magnification TEM image of a porous ZnO nanowire and b) corresponding diffraction pattern; c) high-magnification TEM image taken on the edge of the porous ZnO nanowire; d) low-magnification TEM image of a porous ZnO nanowire with thick Zn_2SiO_4 layers; e) EDS spectra of the Zn_2SiO_4 layer; f–h) high-magnification TEM images recorded from the areas indicated in (d), showing the Zn_2SiO_4/ZnO interface, ZnO core, and Zn_2SiO_4 layer, respectively.

pod structure with one leg longer than the other three presented in Figure 1c.

In accordance with the TEM data, a possible growth mechanism is proposed in Figure 4. Starting from the tin catalyst deposited on the substrate as a thin film, ZnO nanowires are formed by supplying Zn vapor and oxygen from the source material (Figs. 4a,b). The nanowire grows along [0001] and its side surfaces are $\{2\bar{1}\bar{1}0\}$. In a high-temperature region, ZnO nanowires can decompose into the original Zn vapor and O_2 at a local substrate temperature of ~ 600 °C. Meanwhile, Si–O vapor sublimated from the silicon substrate can quickly be deposited on the nanowire surface and diffuse into the ZnO lattice, resulting in the formation of a new phase, Zn_2SiO_4. The electronegativity of Si is 1.9 and that of Zn is 1.65, which are quite close values. Additionally, the atomic size of Si and Zn, 0.117 and 0.133 nm, respectively, are also comparable. Additionally, ZnO and SiO vapor can quickly combine to form a new phase:

$$2\,ZnO + SiO_2 \rightarrow Zn_2SiO_4 \quad (1)$$

The newly formed Zn_2SiO_4 layer tends to have an epitaxial relationship with ZnO in order to reduce the interface lattice mismatch (Fig. 4c). On the other hand, the lattice mismatch between $(0001)_{ZnO}$ and $(001)_{Zn_2SiO4}$ is 14 %, and between $(01\bar{1}0)_{ZnO}$ and $4(010)_{Zn_2SiO4}$ is 9 %. Zn_2SiO_4 tends to form textured islands on the surface of ZnO, but they cannot form a continuous single-crystalline film due to the large lattice mismatch; this results in the growth of epitaxial Zn_2SiO_4 islands on the ZnO surface. The newly formed Zn_2SiO_4 may be more stable than ZnO at the local growth temperature. Therefore, there are open areas on the ZnO surface that are not covered by the Zn_2SiO_4 network. The evaporation of ZnO from the open areas may form the porous interior of the nanowire. The sublimation of ZnO and growth of Zn_2SiO_4 proceed simultaneously and finally result in a high-porosity ZnO nanostructure (Fig. 4d).

It is well known that Zn_2SiO_4 is a green luminescent material and ZnO has a near-UV luminescence. A UV photoluminescence (PL) system was used to characterize the optical properties of the porous ZnO nanowires that are enclosed by Zn_2SiO_4. As shown in Figure 5, a near-UV luminescence peak

ADVANCED MATERIALS

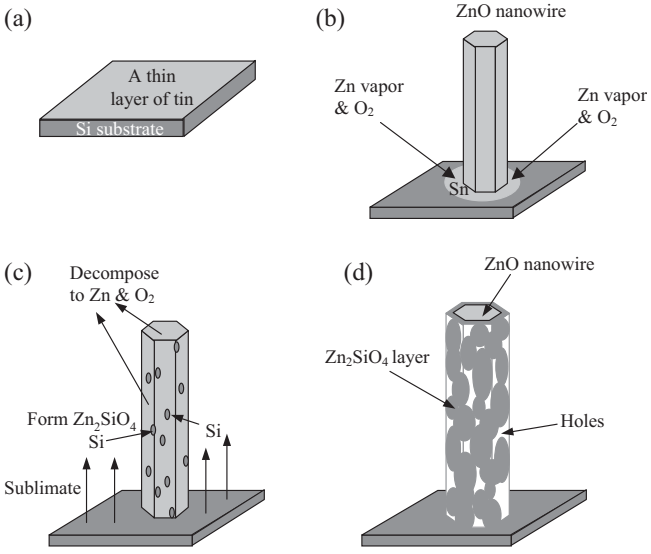

Figure 4. Schematic of the proposed mechanism for growth of high-porosity ZnO nanowires.

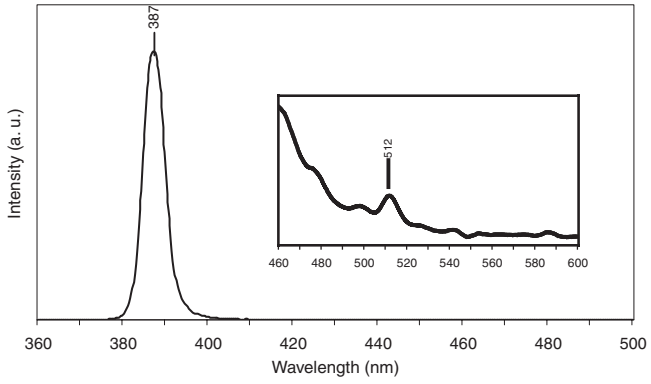

Figure 5. Photoluminescence spectra of high-porosity ZnO nanowires. The inset is an enlarged spectral region showing the luminescence peak contributed by Zn_2SiO_4.

is observed at 387 nm, which is consistent with our previous results on other ZnO nanostructures. Additionally, a small green peak located at 512 nm is also observed (see the inset), which is attributed to Zn_2SiO_4. It was reported that both pure[18] and magnesium-doped[19] Zn_2SiO_4 bulk crystals have a luminescence peak at 525 nm. A shift of the peak to 512 nm in our case is possible owing to the small thickness of the Zn_2SiO_4 layer.

In summary, high-porosity ZnO nanowires were synthesized for the first time using a solid–vapor process on a silicon substrate. The nanowires were single crystals and grew along the [0001] direction. The thermal decomposition of ZnO and the formation of a non-continuous Zn_2SiO_4 network on the surface of the nanowire are the key for forming the high-porosity volume. This technique reveals a new approach for fabricating high-porosity nanowires as well as composite ZnO–Zn_2SiO_4 luminescence materials. Some other complex junctions such as tetrapod sprouts and rib-like arrays were also found. These unique structures exhibit a very high surface-to-volume ratio and are expected to have a high absorptive capacity and particular chemical selectivity that could be applied to filter and sensor systems.

Experimental

The high-porosity ZnO nanowires were synthesized using a solid–vapor process. The ZnO powders (99.9 %) acquired from Alfa Aesar were used as source materials. In a typical experiment, a {111} orientated silicon substrate was cleaned by a 2:1 mixture (by volume) of H_2SO_4 (98 %) and H_2O_2 and a 10 nm thin film of tin was coated onto the silicon substrate using a thermal evaporator with a quartz crystal thickness monitor for obtaining exact tin film thickness. 2 g of ZnO powder was loaded into an alumina boat and placed in the center of an alumina tube in a horizontal tube furnace. The tin-coated silicon substrate was located about 12 cm downstream from the source. Both ends of the tube were water cooled to achieve a reasonable temperature gradient. The tube was first pumped down to 5×10^{-3} torr at room temperature and then heated to 800 °C at a rate of 25 °C min^{-1}. After being held at this temperature for 20 min, the furnace was heated up to 1300 °C at a rate of 20 °C min^{-1}. Meanwhile, a constant flow of Ar gas was introduced at 20–30 sccm to bring the pressure back to 200–300 torr. This condition was held for 30 min to achieve the final nanostructure geometry. The furnace was then shut down and cooled to room temperature under an Ar flow.

The products were characterized by scanning electron microscopy (SEM) (LEO 1530 FEG at 10 kV) and transmission electron microscopy (TEM) (Hitachi HF200 at 200 kV). Energy-dispersive X-ray spectroscopy (EDS) analysis was performed during the TEM measurements. Photoluminescence (PL) measurements were performed at room temperature using a 337 nm N_2 pulsed laser as the excitation light source. The laser repetition rate was 15 Hz, with a 800 ps pulse duration at an average energy of 50 mW.

Received: November 21, 2003
Published online: May 19, 2004

[1] H. Cao, J. Y. Xu, D. Z. Zhang, S. H. Chang, S. T. Ho, E. W. Seelig, X. Liu, R. P. H. Chang, *Phys. Rev. Lett.* **2000**, *84*, 5584.
[2] J. S. Wang, K. M. Lakin, *Appl. Phys. Lett.* **1983**, *42*, 352.
[3] Z. W. Pan, Z. R. Dai, Z. L. Wang, *Science* **2001**, *291*, 1947.
[4] M. H. Huang, Y. Wu, H. Feick, N. Tran, E. Weber, P. Yang, *Adv. Mater.* **2001**, *13*, 113.
[5] P. X. Gao, D. Yong, Z. L. Wang, *Nano Lett.* **2003**, *3*, 1315.
[6] X. Y. Kong, Y. Ding, Z. L. Wang, *J. Phys. Chem. B* **2004**, *108*, 570.
[7] X. Y. Kong, Z. L. Wang, *Nano Lett.* **2003**, *3*, 1625.
[8] M. S. Gudiksen, J. Wang, C. M. Lieber, *J. Phys. Chem. B* **2001**, *105*, 4062.
[9] X. D. Wang, Y. Ding, C. J. Summers, Z. L. Wang, *J. Phys. Chem. B*, in press.
[10] P. X. Gao, Z. L. Wang, *J. Phys. Chem. B* **2002**, *106*, 12 653.
[11] *Nanowires and Nanobelts* (Ed: Z. L. Wang), Kluwer Academic Publisher, Dordrecht, The Netherlands **2003**, Vols. I,II.
[12] E. Kramer, S. Forster, C. Goltner, M. Antonietti, *Langmuir* **1998**, *14*, 2027.
[13] V. Hornebecq, Y. Mastai, M. Antonietti, S. Polarz, *Chem. Mater.* **2003**, *15*, 3586.
[14] A. I. Cooper, *Adv. Mater.* **2003**, *15*, 1049.
[15] S. Takeuchi, H. Iwanaga, M. Fujii, *Philos. Mag. A* **1994**, *69*, 1125.
[16] Y. Dai, Y. Zhang, Z. L. Wang, *Solid State Commun.* **2003**, *126*, 629.
[17] Z. L. Wang, X. Y. Kong, J. M. Zuo, *Phys. Rev. Lett.* **2003**, *91*, 185 502.
[18] X. Xu, C. Guo, Z. Qi, H. Liu, J. Xu, C. Shi, C. Chong, W. Huang, Y. Zhou, C. Xu, *Chem. Phys. Lett.* **2002**, *364*, 57.
[19] Z. G. Ji, L. Kun, Y. L. Song, Z. Z. Ye, *J. Cryst. Growth* **2003**, *255*, 353.

